Case Studies in Construction Materials 17 (2022) e01571

Contents lists available at ScienceDirect

Case Studies in Construction Materials

journal homepage: www.elsevier.com/locate/cscm

Case study

Development of a sustainable binder made of recycled high-performance concrete (HPC)

Dana Daneshvar [a], Teresa Liberto [a], Maria Chiara Dalconi [b], Waltraud Stöllinger [c], Johannes Kirnbauer [a], Agathe Robisson [a,*]

[a] Research Group of Building Materials, Institute of Material Technology, Building Physics and Building Ecology, Faculty of Civil Engineering, Vienna University of Technology (TU Wien), Karlsplatz 13/207-01, A-1040 Vienna, Austria
[b] Department of Geosciences – CIRCe, University of Padua, via G. Gradenigo 6, 35131 Padua, Italy
[c] Mixteresting GmbH, Im Bäckerfeld 19, 4060 Leonding, Austria

ARTICLE INFO

Keywords:
High-performance concrete (HPC)
Recycling
Construction and demolition waste (CDW)
Sustainability
Supplementary cementitious materials
SAOS

ABSTRACT

The high consumption of ordinary Portland cement (OPC) in high-performance concrete (HPC), combined with the growing accumulation of construction and demolition wastes (CDW), raises severe environmental and economic concerns. This study addresses both issues by proposing a novel sustainable binder made of milled recycled HPC (mRHPC). A series of HPC mix designs (R-HPC) was developed replacing OPC by mRHPC (0–100%), and characterized in fresh and hardened states. The residual reactivity of mRHPC was detected using X-ray diffraction, calorimetry, and rheological oscillatory measurements (SAOS). Replacement up to 30% resulted in comparable 28-day compressive and flexural strengths to that of the OPC reference specimen while slightly improving fresh properties. Furthermore, the performance of steel fiber reinforced R-HPC overlays was investigated in repair application, and 30% replacement ratio enhanced the tensile bond strength by a factor of 2.4. The measured improved flow properties and reduced drying shrinkage can explain this remarkable result.

1. Introduction

High-performance concretes (HPC), with a compressive strength above 60 MPa, were developed to provide robust, resilient, and sustainable infrastructures, expanding concrete applications to high-rise buildings, wide-span girders, bridges, and shells [1,2]. Besides developing higher strength, HPCs typically exhibit denser microstructure (solid volume fraction in the fresh state above 0.8) and superior durability performance to normal concrete [3,4]. These properties are mainly linked to their lower water-to-binder (W/B) ratio (0.15–0.25) and higher solid packing (coarse aggregates are replaced with finer components such as quartz sand, quartz powder, and silica fume) [5,6]. The addition of fiber reinforcement (2–3% by volume) can further improve flexural and tensile strengths and provide greater ductility and durability, enabling the construction of lightweight, sustainable filigree concrete members with or even without extra reinforcement [2,7,8].

Despite the advantages of HPC, there are still standing challenges [9]. The growing world population and urbanization turn the construction sector into one of the largest consumers of natural resources. The exploitation of 32–50 billion tons of river sand per year combined with the yearly production of over 4 billion tons of cement create severe environmental issues impacting the ecosystem

* Corresponding author.
E-mail address: agathe.robisson@tuwien.ac.at (A. Robisson).

https://doi.org/10.1016/j.cscm.2022.e01571
Received 2 September 2022; Received in revised form 11 October 2022; Accepted 12 October 2022
Available online 13 October 2022

preservation. Mining, shortage of raw natural materials, and greenhouse gas emissions [10–12] all contribute to this disruption. The production of cement indeed accounts for 12–15% of the total industrial energy use and contributes to 5–8% of all anthropogenic CO_2 emissions [13]. The cement technology roadmap [14] calls for a challenging 24% reduction of CO_2 emissions (in cement industry) by 2050. In parallel, the massive generation of construction wastes results in further ecological, environmental, and economic challenges. In Europe alone, more than 850 million tonnes of construction and demolition waste (CDW) are generated every year, amounting to around 40% of all waste [15]. A large portion of these CDWs is disposed in landfills without further recovery [16]. Nowadays, recycling is regarded as one of the most viable CDW management strategies, aiming at turning wastes into cost-effective and high-quality secondary building materials [17]. The revised Waste Framework Directive from the European Union (EU 2018/851) sets a mandatory target for the recovery of CDW waste at 70% [18].

In this framework, the production of eco-friendlier HPCs has been targeted using two main approaches namely recycled concrete aggregates (RCA) [19–22] and supplementary cementitious materials [23–26]. Targeting a sustainable HPC with a reduced amount of natural aggregates (NA), Pedro et al. investigated the performance of coarse and fine recycled aggregates obtained from rejected HPC precast elements with compressive strength of 75 MPa [27]. They reported that this type of high-performance RCA (HP-RCA) provided similar fresh and hardened mechanical properties to that of reference specimen made with NA. Their ultrasonic pulse velocity showed microstructures free of voids and cracks, explaining this result. Andreau and Miren [20] assessed the influence of the RA source concrete strength (using three types: 40, 60 and 100 MPa compressive strength) on the physical, mechanical, and durability properties of the high-performance recycled aggregate concrete (RAC). They could match the mechanical properties (compressive strength) of concrete prepared with NA when using RCA sourced from concrete having a compressive strength of at least 60 MPa. Pedro et al. [28] studied the durability of HPC specimens incorporating HP-RCA. Although the HP-RACs exhibited acceptable resistance to chloride penetration, water absorption, and carbonation depth (less than 1 mm), the high porosity of the RCAs is still a matter of concern due to high oxygen permeability (6 times higher) and water absorption by capillary (38–55%) compared to that of reference concrete. The addition of fine RCA (0–4 mm) was showed to have a detrimental effect on the HP-RAC mechanical properties but did not degrade its freeze–thaw internal cracking resistance [29]. This result was attributed to the higher porosity of fine RCA and hence better dissipation of hydraulic pressure. Bogas et al. [30] investigated mortars incorporating low-carbon recycled cement (RC) obtained from thermally activated (650°C) and ground well-hydrated cementitious wastes. They found that a replacement by up to 20% had insignificant effect on the mechanical properties. In the same study, the produced mortars with 100% replacement of OPC resulting in RC that exhibited about 20% of the compressive strength of the reference samples (OPC). This is a clear indication of the residual reactivity of their heat-treated RC. Another promising approach consisted in incorporating RAs in cement raw mills. Authors recommended keeping the incorporation rate of RAs in cement raw meals below 5%, a rate that could be increased depending on RAs chemical composition, the cement type and the cement quarry composition [31]. Further investigations revealed that the RC obtained from cement and concrete wastes can show appropriate hydration capacity and promote microstructure refinement, enabling up to 15% replacement of OPC with RC without detrimental impact on concrete durability [32]. Moreover, workability, time-dependent properties (shrinkage, creep) and structural performance of the developed mixtures are still areas of concern. For instance, the addition of recycled concrete powder (RCP) leads to a decrease by up to 22% in the initial fluidity of the RCP mortars, reducing the compactness of the mortar and increasing its porosity [33]. Moreover, the increased drying shrinkage (20–80%) may restrict the application of RAC in massive concrete structures that are more sensitive to deformation and cracking [34,35]. The current study proposes a novel binder made of milled recycled high-performance concrete (mRHPC) that could partially replace the ordinary Portland cement (OPC) binder. The low water-to-binder (W/B) ratio of high-performance concrete (HPC) results in a lower hydration rate than in conventional concrete, leading to a significant content of unhydrated clinker particles in the set concrete, even after years [36,37]. This, combined with the high cement content in HPC/UHPC (400–1100 kg/m^3 versus 200–400 kg/m^3 in normal concrete (NC)), makes it a great candidate for its use, after milling, as a binder. Considering this, mRHPC provides a benefit not only in reducing cement consumption but also in reusing CDW (in this case demolished HPC). It is also important to note that HPC concrete is rarely demolished due to its weak performance. Although HPC structures are designed to last long, their demolition is often driven by natural disasters, evolving urban designs, updated architectural needs, and so on. The precast industry also produces a source of HPC wastes. Given precast strict quality control, growing amounts of HPC wastes have been reported [27]. Crushing and recycling these HPC wastes were shown to be beneficial. It is therefore essential to integrate recovery solutions into the design and, doing so, avoid the accumulation of demolished HPC/UHPC, whose potential as a binder, as discussed here, should not be wasted. The authors think it is important to provide knowledge before the need to recycle HPC is overwhelming.

In this work, a series of R-HPC (HPC prepared with recycled HPC) mix designs were prepared, in which the OPC was partially or fully replaced with mRHPC, and experimentally characterized. The residual reactivity of mRHPC powder was first estimated through a combination of X-ray powder diffraction (XRPD), calorimetry, and rheological oscillatory (small amplitude oscillatory shear -SAOS-) measurements. R-HPC mixture properties were then measured in their fresh state using mini V-funnel flow and mini slump flow cone spread, as well as in their hardened state at 1 day, 7 days, and 28 days using three-point bending and compression tests. Furthermore, the use of such materials as overlays in repairing/strengthening applications was considered. To this end, and given the prevalence of fiber-reinforced high-performance concretes (FRHPC) in repairing applications [38–40], the effect of steel fiber inclusion on the mechanical properties and bond performance of the developed R-HPC materials was also studied. This work, overall, aims at bringing a deeper insight into mRHPC as a cementitious binder and maximizing its use as OPC replacement while maintaining comparable fresh and hardened properties.

2. Materials and methods

2.1. Materials

The mRHPC was obtained through a multi-step recycling process as shown in Fig. 1. In this study, the HPC fractured beams were selected to be recycled. The original beams had a surface dimension of 80×12 cm^2 with an average thickness of 4 cm. They were exposed to atmospheric environmental conditions for two years. These beams contained carbon fabrics, were originally prepared with a W/B ratio of 0.3, and had a total original unhydrated cement content of 24 wt%. The W/B ratio was calculated, in the whole document, as the ratio of the sum of pure water and water contained in SP and consistency holder, and divided by the total mass of OPC, mRHPC, and silica fume. The beams were broken into smaller pieces and the remaining fabric was removed. The HPC pieces were then further crushed using a jaw crusher machine to reach a maximum size of 5 cm. The crushed samples were then sieved and the particles passing through the 63 μm sieve were collected for the milling process. Finally, the passed 63 μm particles were milled by 50 steel balls (diameter 20 mm) in a ceramic container.

Matching mRHPC particle size distribution (PSD) to that of OPC was important to prevent significant changes in the packing density and microstructure of the mixtures. To this end, various milling times (1, 2, 3, and 4 h) were considered and their impacts were assessed based on the PSD analysis performed on the obtained mRHPC powders. PSD measurements of all solid components were performed using a MALVERN Mastersizer-3000 (laser diffraction spectroscopy technique). The measurements were repeated three times for each sample and gave negligible scatter. As presented in Fig. 2, there was no remarkable decrease in particle sizes after increasing the milling time to more than two hours. Considering the cost and energy of milling, a two-hour duration was selected as optimal in this study. The required energy for the crushing and milling processes was not quantitively analyzed but was considered to be smaller than the energy associated with clinker milling in OPC production [41]. Therefore, in regard to grinding, the replacement is neutral or slightly beneficial. The density of the obtained dry mRHPC powder was measured with a pycnometer and the average value of three measurements equaled 2.43 g/cm^3. The comparison between the composition and early reactivity of mRHPC and OPC powders is discussed in Section 2.2.

Combined with mRHPC, ordinary Portland cement (CEM I 52.5 N) from Lafarge and silica fume from ELKEM (Microsilica 940 U, CAS number 69012–64–2) were also used, forming the binder of the R-HPC mixtures. Their specific gravities were 3.1 and 2.3 g/cm^3, respectively. To enable the low W/B and maintain workability, a carboxylether-based superplasticizer (MasterGlenium ACE430) and a consistency holder (MasterSure 911), sourced from BASF, were employed. The quartz sand and quartz powder are typical inert constituents used to reach optimum packing density, reducing the initial porosity of the mixture and increasing the compressive

Fig. 1. Recycling process of high-performance concrete (HPC) to obtain mRHPC.

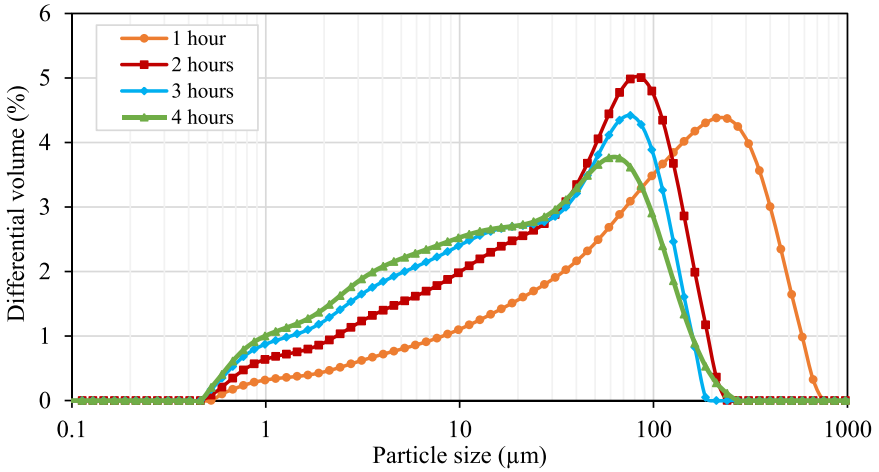

Fig. 2. Particle size distribution of mRHPC after various milling times. Each plot presents an average of three distinct measurements. The error bar is smaller than the size of the marker and therefore not visible.

strength of the hardened concrete. The quartz sand and quartz powder were obtained from Quarzwerke Austria GmbH company and have a density equal to 2.65 g/cm^3. As an inert filler, the chemical purity of quartz powder is of great importance. The analysis showed that it mainly contains SiO_2 (97 wt%) and Al_2O_3 (1.6 wt%). For the production of quartz powder with a defined grain size, separation processes were performed in addition to iron-free grinding. By combining grinding and classifying technology, it is feasible to produce quartz powders with a grain size down to 1 μm. The PSD results for all powders are presented in Fig. 3 and Table 1.

Steel fibers are often used to mitigate the brittle failure of HPCs [42]. They enhance the tensile strength and ductility of the concrete mixture through a crack-bridging mechanism, resulting in the formation of multiple micro-cracks instead of a large crack [43]. The degree of improvement depends on the fiber characteristics (geometry, length, surface morphology) as well as on their interaction and interlocking with the concrete matrix [7,44]. To assess the effect of fiber inclusion on the mechanical performance of the developed R-HPC, straight steel fibers with a length of 12.5 mm and a diameter of 0.175 mm were used.

2.2. Estimation of early residual reactivity of mRHPC

In order to estimate the early residual reactivity of the mRHPC, several tests were performed on the mRHPC powder, both dry and combined with distilled water to form a paste. In particular, the mRHPC powder was tested via X-ray powder diffraction (XRPD) to obtain its mineral composition, with a special focus on the reactive phases (i.e., unhydrated phases containing calcium). The pH of the mRHPC suspension (at W/B=2) was measured using a pH-meter (SevenCompact S213 Mettler Toledo) with an electrode optimized for a highly alkaline solution, inserted into the suspension immediately after mixing the mRHPC powder and water by hand. The measurement was continued for 4 h under constant magnetic stirring. The pH value increased from 12.3 to 12.5 in the first 5 min and remained rather constant for the rest of the experiment. In comparison, the pH value of OPC concrete was in the range of 12.5–13 [45,46]. As carbonation and steel corrosion mostly occur when the pH value goes below 11.5 [47], there was, therefore, not any concern when OPC is replaced with mRHPC. The properties of mRHPC and OPC in their fresh state were also compared. Their heat of hydration was quantified with the aid of a custom-built semi-adiabatic calorimeter, using multichannel Omega (Norwalk, US) thermocouples.

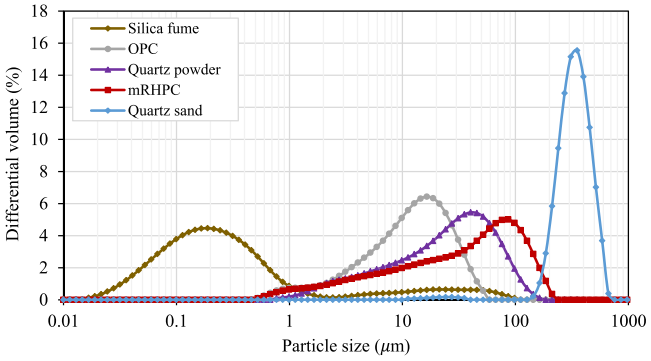

Fig. 3. Particle size distribution of R-HPC components (differential distribution). Each plot presents an average of three distinct measurements. The error bar is smaller than the size of the marker and therefore not visible.

Table 1
Summary of particle size distribution of R-HPC components.

Constituents	value (μm)		
	D10	D50	D90
Silica fume	0.053	0.21	8.7
OPC (CEM I 52.5 N)	2.6	11.7	27.5
Quartz powder	3.7	24.2	68.5
mRHPC	2.9	34.4	112
Quartz sand	205	315	460

The early cohesion of the pastes and their evolution in time were measured via small oscillatory rheological measurements (SAOS) using an Anton-Paar MCR 302 torque-controlled rheometer.

2.2.1. X-ray powder diffraction (XRPD)

The mineral composition of the mRHPC sample was investigated via XRPD using a PANanalitycal X′Pert Pro diffractometer operating in the reflection mode with Co-Kα radiation and X′Celerator detector. The accelerating voltage and current were 40 kV and 40 mA, respectively. Diffraction data were collected in the 5–85° 2θ range with steps of 0.017°. The diffraction patterns highlighting the diffraction peaks of the clinker phases of OPC and mRHPC are shown in Fig. 4. The amount of unhydrated products can be quantitatively analyzed by considering the peak intensity of the reactive calcium-rich phases such as C_3S (alite), C_2S (belite), C_4AF (alumino-ferrite phase) and by applying the Rietveld method [48]. Rietveld analysis was conducted using the Topas software and a known amount of internal standard zincite (ZnO) that was added to the powder sample for quantifying the amorphous fraction. As shown in Table 2, the mass percentage of C_3S, C_2S, and C_4AF were 2.9, 1.5, and 1.1, respectively. Thus, in total, approximately 6.5 wt% of the mRHPC were still unhydrated clinker and thus were identified as the cause of the residual reactivity of this powder. The mRHPC also contained mineral phases such as phyllosilicates, feldspar, quartz, dolomite, and calcite linked with the aggregates used in the HPC beams. In fact, they were prepared with commercial calcite-based sand (0–1 mm) and limestone powder, explaining the high percentage of calcite/dolomite in the mRHPC powder. The OPC, instead, showed a typical composition of a C_3A-free cement: 66.1% of C_3S, 12.4% of C_2S, and 12.6% of C_4AF, together with 6.6% of $CaSO_4$ and 1.6% of CaO.

The total amount of reactive phases (C_3S, C_2S, and C_4AF) was therefore equal to 6.5 wt% for the mRHPC and 91.1 wt% for the OPC, i.e., a ratio of 14. In fact, the early reactivity of the two cementitious pastes can be mainly attributed to C_3S (which reacts immediately after contact with water) and C_2S (~hours), while C_4AF reacts more slowly in time (~days) [48]. It must be highlighted that the mRHPC powder contains amorphous phases created and formed during the hydration process. These amorphous phases (22.5 wt%) cannot be detected by the XRPD method. However, the clinker calcination results in a highly crystalline microstructure in OPC, allowing to identify almost all phases by the XRPD technique.

2.2.2. Calorimetry

Calorimetry tests were carried out both on OPC (W/B=0.4) and mRHPC (W/B=0.3) pastes. The powder content of the two pastes was chosen to have a similar consistency (see Section 2.2.3). The pastes were obtained by mixing distilled water with the dry powder using an overhead stirrer (IKA) for three minutes at the maximum speed (800 rpm). Immediately after mixing, the paste was inserted into an isolated container and placed into an insulated chamber, and thermocouples were introduced to measure the sample and chamber temperatures. Both the rate of heat evolution and cumulative heat of hydration were calculated based on the mass of OPC or mRHPC dry powders (Figs. 5 and 6). As can be seen in Fig. 5, the peak of heat flow before 10 h likely indicates the reaction of residual calcium-rich phases (mainly C_3S and C_2S observed in the XRPD method) existed in the mRHPC powder. Moreover, the gradual increase of generated heat over 2 days also shows the reaction kinetics of the mRHPC, confirming further the presence of unhydrated phases in

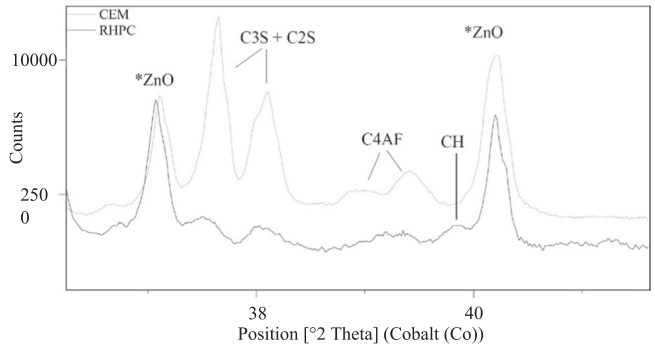

Fig. 4. X-ray diffraction patterns of OPC (CEM I 52.5 N, gray line) and mRHPC powder (black line). 2θ range highlighting diffraction peaks of clinker phases. C_3S, C_2S, C_4AF, and CH refer to tricalcium silicate ($3CaO.SiO_2$), dicalcium silicate ($2CaO.SiO_2$), tetracalcium aluminoferrite ($4CaO.Al_2O_3.Fe_2O_3$), and calcium hydroxide ($Ca(OH)_2$), respectively. *ZnO: zincite was added as an internal standard to quantify amorphous content.

Table 2
Rietveld quantitative phase analysis results. Numbers in parentheses refer to errors as calculated by Topas and are purely related to the mathematical fit. Am-Unkn refers to amorphous and unknown phases not described by a crystalline structural model.

Phase Name	wt% in original sample	
	OPC	mRHPC
C_2S beta	12.4(1)	2.9(1)
C_3S monoclinic (NISHI)	66.1(5)	1.5(1)
C_4AF	12.6(1)	2.1(1)
Anhydrite $CaSO_4$	6.6(1)	–
Portlandite CH	0.7(1)	1.2(1)
Lime (CaO)	1.6(1)	–
Periclase (MgO)	< 1	–
Calcite	–	33.0(1)
Ettringite	–	< 1
Dolomite	–	13.0(1)
Quartz	–	18.7(1)
Muscovite	–	2.8(1)
Chlorite	–	0.8(1)
Feldspar	–	1.2(1)
Am-Unkn	–	22.5(5)

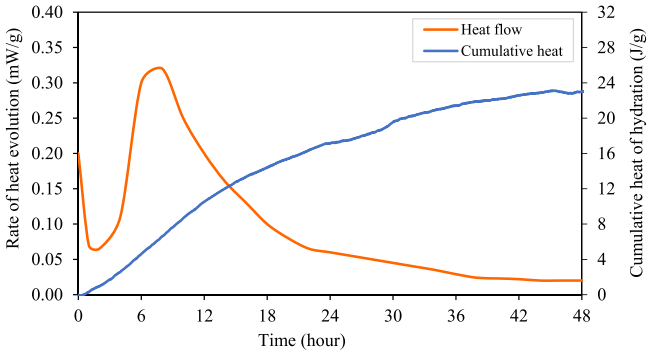

Fig. 5. Heat flux and cumulative heat of hydration of mRHPC, gained from semi-adiabatic calorimetry measurement.

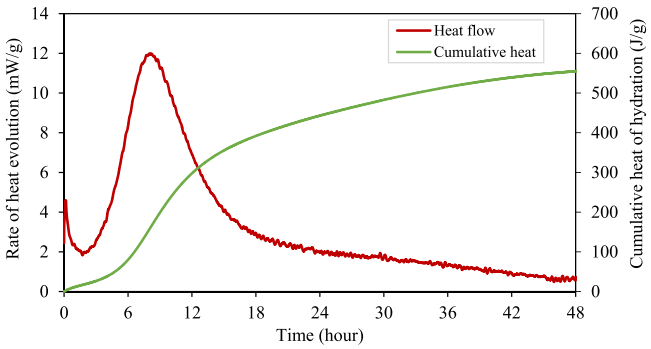

Fig. 6. Heat flux and cumulative heat of hydration of OPC, gained from semi-adiabatic calorimetry measurement.

the original demolished HPC. After 2 days, the cumulative heat of hydration of mRHPC amounted to 23 J/g while it reached 555 J/g for the OPC, i.e., a ratio of 24. In comparison, the relation of the masses of the reactive products (weighted before the test), in the two samples was about 10. This difference can be attributed to the additional heat of hydration in the OPC produced by the highly exothermic reaction between anhydrite and calcium aluminate phases (forming AFm and ettringite) [48].

2.2.3. Rheology

Small amplitude oscillatory rheology (SAOS) has been used to describe the structural buildup of cement pastes, tracing what can be defined as cohesion (storage modulus G′) in time [49–54]. G′ describes the elastic contribution of the complex viscoelastic response of a

paste under shear in its linear regime [55]. The characterization of G′ in the early stage provides insight into the initial cohesion of the paste and its reactivity progress (the dissolution-precipitation process leading to hydration) [56]. SAOS measurements were performed for both mRHPC (W/B=0.3, corresponding to a volume fraction of 0.58) and OPC pastes (W/B=0.4, corresponding to a volume fraction of 0.45) using a rheometer (MCR 302, Anton Paar) equipped with a serrated plate-plate geometry, with an upper diameter of 25 mm (PP25/P2). The W/B was chosen to have a similar initial G′. The gap between the plates was optimized for both pastes to minimize disruption during placement in a range between 1.7 and 2.5 mm. The pastes were obtained by mixing distilled water and the powder using an Ultra Turrax mixer (IKA) at the maximum rotation speed (6000 rpm) for three minutes. The paste was then immediately placed on the rheometer, and the test was started. In order to measure the structural buildup within the paste without damaging it, a small amplitude deformation ($\gamma = 0.0005\%$) with a frequency of 1 Hz was imposed for one hour at a constant temperature of 20 °C. Moreover, a moisture chamber was used to prevent evaporation. It must be highlighted that the imposed amplitude deformation was within the linear viscoelastic regime of the paste [52] and the normal force evolution was continuously monitored to confirm the contact between the paste and the upper plate. The measurements on the two samples (mRHPC and OPC) were repeated three times to check the reproducibility of the results. The data presented here was rescaled in time and G′ to discard the first two minutes of the test. This time seemed to be the one needed for the paste to recover from the placement process, and the corresponding measurements are noisy [52]. Furthermore, the time limit of the test was set to one hour. This limit was chosen due to the development of high structuration/hydration related normal forces in the paste, and to avoid potential artifacts linked to the later water evaporation process. The evolution of the rescaled storage modulus G′ as a function of time is presented for both mRHPC and OPC pastes in Fig. 7. The G′ increased as a function of time for both pastes, showing a structural buildup connected with the early hydration process. The G′ for pure cement at a solid volume fraction of 0.45 reached 1560 kPa, and the one of mRHPC at a solid volume fraction of 0.58 achieved 542 kPa, after one hour. This early hydration corresponds to the initial dissolution of cement grains and the precipitation of calcium silicate hydrates (C-S-H) [56,57]. However, the evolution rate (slope) of G′, which is linked to the amount of reacting calcium-rich phases, (i.e., mainly C_3S in the first hour) differed in the two studied pastes. As expected, the OPC revealed a higher growth rate owing to the abundance of reactive phases (mainly C_3S). The observed growth rate of mRHPC, while less significant, confirms the immediate contribution and reactivity of the unhydrated phases (as observed via XRPD) when they get in contact with water.

2.3. Preparation of R-HPC mixtures

R-HPC mixtures containing different percentages of mRHPC were prepared and characterized. A reference HPC mixture (R0) was designed with OPC only, while in other mixtures a growing volume percentage of cement was replaced with mRHPC. Each R-HPC mixture is denoted with the "RX" label where the X represents the replacement percentage (vol%) of reference OPC content. All other constituents of the cast mixtures were kept constant. The mix design is presented in Table 3. A new water to binder ratio (W/B_{eff}) was defined as the ratio of pure water plus water contained in SP and consistency holder divided by the total mass of OPC, silica fume, and 6.5 wt% percent of mRHPC (i.e., reactive fraction measured via XRPD).

The EIRICH intensive mixer type R02Vac was employed to prepare the mixtures. The dry components were first added to the 5 L mixing pan and dry-mixed for 90 s with a rotational speed of 660 rpm. This step was performed to deagglomerate and uniformly distribute the dry particles. While mixing, the liquid constituents (pre-mixed water, superplasticizer, and consistency holder) were poured into the mixing pan through an external vessel. The torque induced by the mixer was monitored. Upon adding the liquid part, the torque immediately increased and reached its peak within a few minutes, followed by a gradual decrease over time. In this study, the mixing was continued for 8 min, ensuring the induced torque reached a constant value. Then, a part of the R-HPC mixture was collected for fresh state characterization (described in Section 2.5.1) and the rest was immediately poured into standard $4\times4\times16$ cm^3 prismatic steel molds. The filled molds were covered with plastic sheets and kept in the lab ambient conditions (average temperature of 23 °C and relative humidity of 50%). After one day, the samples were demolded and cured further in the same condition until achieving the ages of 1, 7, and 28 days, respectively. Fiber-reinforced specimens were prepared as above, but steel fibers (2% by volume of mixture) were added during mixing right after the addition of the liquid constituents.

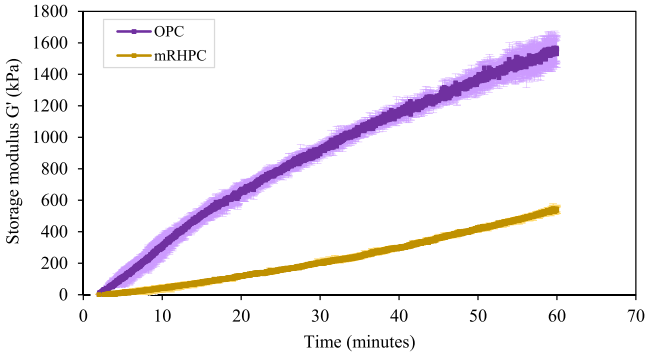

Fig. 7. Evolution of the storage modulus (G′) as a function of time measured by the rheometer. Error bars represent standard deviation from three distinct measurements.

Table 3
Mix proportions of R-HPC.

Constituents	Amount (kg/m^3)						
	R0	R10	R20	R30	R40	R50	R100
Cement (CEM I 52.5 N)	772.2	695.0	617.7	540.5	463.3	386.1	0.0
Silica fume	154.4	154.4	154.4	154.4	154.4	154.4	154.4
Quartz powder	308.9	308.9	308.9	308.9	308.9	308.9	308.9
Quartz sand	848.0	848.0	848.0	848.0	848.0	848.0	848.0
mRHPC	0.0	60.6	121.1	181.6	242.1	302.5	605.3
Superplasticizer	34.7	34.7	34.7	34.7	34.7	34.7	34.7
Consistency holder	15.4	15.4	15.4	15.4	15.4	15.4	15.4
Water	179.6	179.6	179.6	179.6	179.6	179.6	179.6
W/B_{eff} Ratio	0.23	0.25	0.27	0.30	0.34	0.38	1.11
CEM replacement [vol%]	0	10	20	30	40	50	100

2.4. Preparation of FRHPC-NC composites

A series of concrete composites made of NC substrate and fiber-reinforced high-performance concrete overlay (FRHPC-NC) was cast to evaluate the structural performance of the developed recycled concrete in repair applications. NC substrates ($25\times25\times6$ cm^3) were prepared in advance (1 year old), sandblasted, and humidified with a wet sponge to reach SSD conditions right before the FRHPC overlay was poured. The overlay quantity was added to reach a final thickness of 4 cm [58]. These composites were cured in the climate chamber with a controlled temperature of 23 ± 1 °C and relative humidity of 90 ± 3%. Fig. 8(a) shows an example of the final shape of the demolded FRHPC-NC composites. After 28 days of curing, prism samples ($5\times5\times10$ cm^3) were cut out of the FRHPC-NC composite to perform the direct tension test (see Fig. 8(b)).

2.5. Characterization of R-HPC mixtures

2.5.1. Fresh state properties

The impact of mRHPC replacement on the fresh state properties and workability of the R-HPC mixture was evaluated by mini slump flow cone and mini V-funnel flow tests. In the mini slump cone test, the cone was placed on a pre-wetted horizontal surface and filled with the mixture. Then, the cone was lifted upward and the mixture flowed and spread over the surface by gravity-induced forces. The average diameter of the spread was reported as the slump flow index, representing deformability and yield stress. In the mini V-funnel flow test, after filling the 1.1 L funnel with the mixture, the trap door at the bottom of the funnel was released. The corresponding time required by the mixture to completely empty the funnel was reported as the flow time, linked to the viscosity of the mixture.

2.5.2. Mechanical properties

Flexural and compressive strengths of the hardened R-HPC were measured by three-point bending and compression tests at the ages of 1,7, and 28 days. The tests were performed using a Zwick 250 kN testing machine and the vertically applied load was measured by a

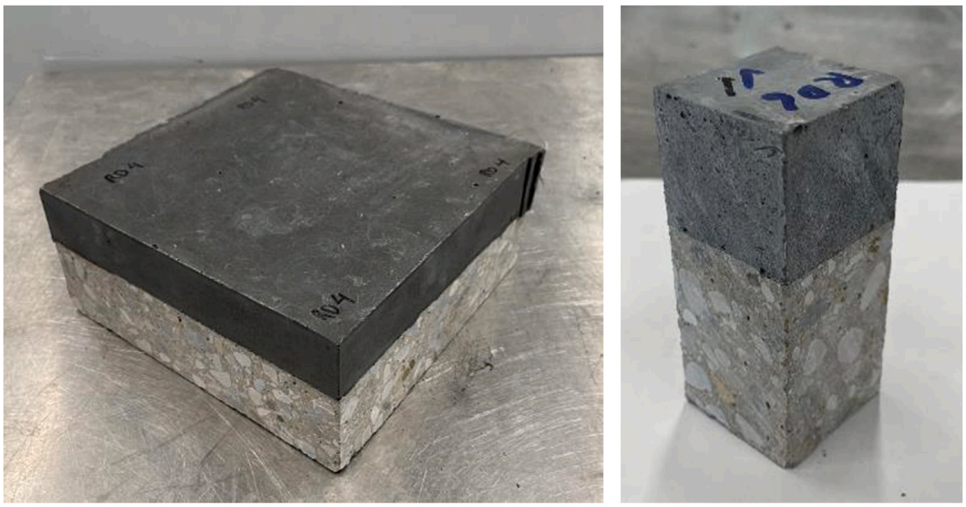

(a) **(b)**

Fig. 8. Examples of prepared specimens; (a) FRHPC-NC composite, (b) cut sample for direct tension test.

100 kN load cell. The prisms ($4\times4\times16$ cm^3) were placed with a span of 10 cm and loaded at a rate of 15–60 N/s, depending on the age of the specimens. The loading rates were selected based on the recommendation of ÖNORM EN 206. The peak load was used to calculate flexural strength. The resultant halves were then employed in the compression test such that each half was placed between two steel plates (4×4 cm^2) and subjected to the compressive load with a loading rate in the range of 1–2.5 MPa/s, depending on the age of the specimen (ÖNORM EN 206). The peak load was used to calculate the compressive strength.

Tensile bond strength of the FRHPC-NC samples was measured using the direct tension test. As depicted in Fig. 9, the tension load was applied perpendicular to the interface through two steel dollies glued to both sides of the sample. The test was conducted with a monotonic loading rate of 0.05 MPa/s. Three replicates for each type of mixture were prepared and tested. To enforce the failure occurrence at the interface, a notch of depth 5 mm was carefully sawed along the interface on all sides of the samples, reducing the interface surface area to 4×4 cm^2. All failures indeed occurred at the interface so that the interfacial tensile bond strength could be calculated for all samples.

2.5.3. *Drying shrinkage measurements*

The magnitude of free drying shrinkage of the fiber-reinforced R-HPC prisms ($4\times4\times16$ cm^3) was measured using mechanical dial gauges with a resolution of 0.001 mm. The samples were demolded one day after casting and then transferred into a climate chamber with a controlled temperature of 23 ± 1 °C and relative humidity of 90 ± 3%, similar to curing conditions of all FRHPC-NC composites described hereafter. The length variations of the samples were then monitored daily and the values were converted into a shrinkage strain.

Fig. 9. Examples of FRHPC-NC samples under tensile bond test.

3. Results and discussion

3.1. Characterization of R-HPC mixtures

3.1.1. Fresh state properties

The effects of replacing OPC by mRHPC on the slump flow and V-funnel flow time of the mixture are presented in Fig. 10. Except for R0 and R100 samples, the values of slump flow and flow time were respectively in the range of 28–30 cm and 14–15 s for all samples. The partial replacement of cement by mRHPC (up to 50%) lead to slight improvements in workability. This enhancement can be attributed to the mRHPC coarser particle size compared to the OPC, which reduces the amount of water required to wet the mRHPC, leading to a cement paste with higher fluidity [59]. Moreover, replacing OPC by a less reactive material (mRHPC), resulted in reduced inter-particle attraction, weaker cohesion, and hence higher dispersion of cement particles (as shown in rheology, see Section 2.2.3). However, fully replacing OPC by mRHPC decreased workability. In this case, the change in packing (and therefore amount of required water to fill the space), as well as the porosity of mRHPC particles, may dominate over the effects mentioned above, and lead to unfavorable workability. In fact, additional water (5% by mass of water) had to be added to R100 to achieve a comparable slump flow and V-funnel flow time.

3.1.2. Mechanical properties

The effect of cement replacement by mRHPC on the sample average compressive strength is plotted in Fig. 11. The compressive strength of the reference sample (without mRHPC) reached 121 MPa after 28 days of curing. While a 10% replacement ratio did not significantly alter the compressive strength, a 30% replacement ratio decreased it by about 10%. Interestingly, the R100 sample (where OPC was fully replaced with mRHPC powder), still developed a 28-day compressive strength of 22.5 MPa. This clearly revealed the remaining reactivity of the mRHPC powder, attributed to the contribution of unhydrated particles. A typical post-mortem sample for the R100 is shown in Fig. 12. The 6.5% of reactive phases in mRHPC generated a compressive strength of 22.5 MPa while OPC with 91% of reactive phases exhibited a strength of 121 MPa. Owing to the similar trends and changes of compressive strength at different testing ages (1, 7, and 28 days), it can be concluded that the impact of the mRHPC replacement was similar both on early-age and long-term mechanical properties.

Flexural strength results are shown in Fig. 13. The reference specimen (R0) had a 28-day flexural strength of 17.6 MPa. Upon replacing OPC by up to 40% mRHPC, only negligible changes in the 28-day flexural strength were observed. Given the data variability, it can be concluded that samples R0 to R40 exhibited similar flexural strength results. However, at early ages, increasing the mRHPC replacement ratio from 0% to 40% led to a decrease in 1 and 7-day strength by 33% and 25%, respectively. Here again, the R100 specimens still exhibited a 28-day flexural strength of 6.6 MPa. This is consistent with the compressive strength results and the observation of the XRPD measurement, demonstrating the residual reactivity in the mRHPC powder. Comparing the compressive and flexural strength results demonstrated that mRHPC replacement has less impact on the flexural strength of the samples.

3.1.3. Fiber inclusion

The influence of mRHPC replacement was also assessed in HPC containing common straight steel fibers (with a length of 12.5 mm and a diameter of 0.175 mm). As shown in Figs. 14 and 15 (where F stands for fiber), the inclusion of mRHPC powder (up to 30%) into steel fiber-reinforced R-HPC did not remarkably affect the compressive and flexural strengths of the specimens (i.e., less than 10% reduction). In general, and compared to the unreinforced specimens, the fiber-reinforced R-HPC specimens lost less compressive and flexural strengths upon inclusion of mRHPC. This provides the opportunity of extending OPC replacement (up to 50%) by mRHPC while maintaining comparable mechanical properties.

The strength ratio of the fiber-reinforced R-HPC specimens to the non-reinforced R-HPC specimens at the age of 28 days was also calculated. In fact, the mechanical properties of fiber-reinforced concrete composites not only depend on the fiber parameters, but are also closely related to the matrix strength and fiber-matrix interaction [60]. A matrix with inferior tensile and shear strengths may change the damage mechanism from a strain-hardening mechanism to a failure in the matrix with a diminished role of fibers. As shown in Fig. 16, compressive and flexural strengths of all samples increased by at least 35% as a result of steel fiber inclusion (2% vol.). Considering similar increase in mechanical properties of FRHPC samples containing different mRHPC replacement ratios, it can be concluded that the employed approach (replacing the OPC with mRHPC up to 50%) did not negatively affect the contribution of aforementioned mechanisms.

The inclusion of fibers improved the compressive strength as much or even slightly more than the flexural strength. This can be attributed to two distinct causes related to fiber content and size effect. Ren et al. reported a threshold in volume content of straight steel fiber above which a remarkable increase in flexural strength was observed [61]. They reported, however, that changing the fiber content had less impact on the compressive strength. In the composites presented here, although satisfactory compressive and flexural strength results were obtained using 2% of steel fibers (by volume), a sharp increase in flexural strength may be reached upon using higher volume content of fibers. Moreover, the compressive strength tests were performed on half prisms of size 4×4 cm^2, smaller than typical samples used in compression test campaigns (10×10 cm^2 or 15×15 cm^2). This may lead to both higher compressive strength results and a potentially overrated compressive strength enhancement due to fibers (Fig. 17).

3.1.4. Drying shrinkage

The free drying shrinkage of the steel fiber reinforced R-HPC samples used for the FRHPC-NC composites was measured over close to 100 days after casting. Fig. 18 shows the impact of cement replacement on the cumulative drying shrinkage value of fiber-reinforced

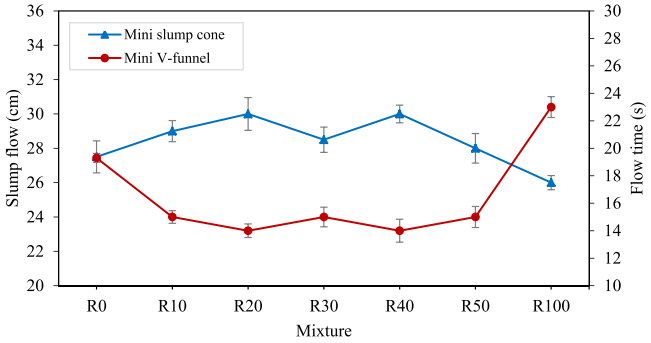

Fig. 10. The results of mini slump flow cone and mini V-funnel flow tests for R-HPC mixtures with replacement percentage of OPC by mRHPC. The error bar represents the standard deviation from three distinct measurements.

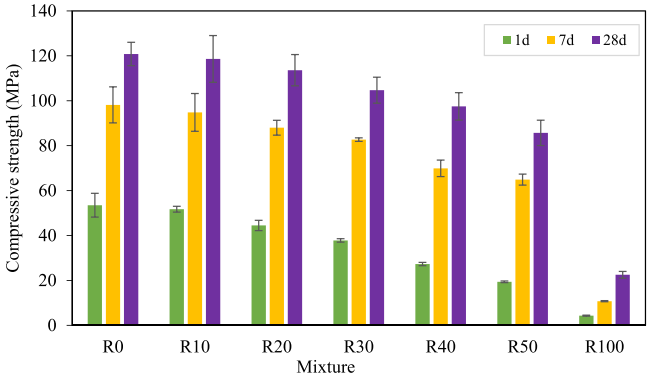

Fig. 11. Compressive strength of the R-HPC mixtures with different replacement ratios tested after 1, 7, and 28 days. The error bar represents the standard deviation from three distinct measurements.

Fig. 12. Post-mortem compression test sample made of 100% mRHPC (R100).

R-HPC samples. Replacing OPC with mRHPC led to a decrease in drying shrinkage. For instance, the F-R50 samples exhibited a drying shrinkage of 274 microstrain (μm/m) at 100 days. This is approximately 20% lower than that of the reference sample (F-R0). The decrease in drying shrinkage can be mainly attributed to the reduction of use of OPC and lower specific surface areas of mRHPC [62].

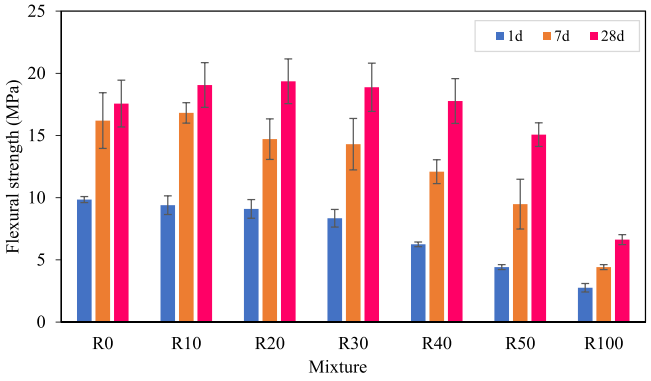

Fig. 13. Flexural strengths of the R-HPC mixtures with different replacement ratios tested at ages of 1, 7, and 28 days. The error bar represents the standard deviation from three distinct measurements.

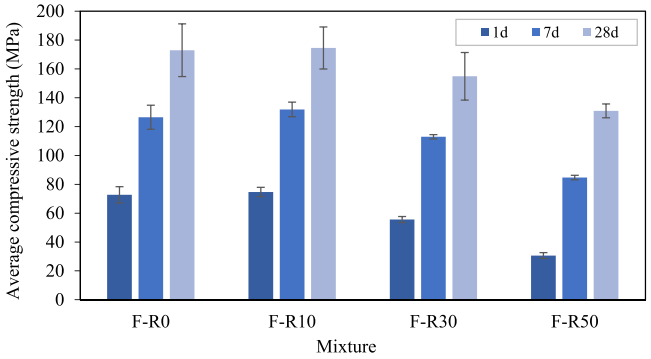

Fig. 14. Compressive strengths of the fiber-reinforced R-HPC mixtures with different replacement ratios tested at ages of 1, 7, and 28 days. The error bar represents the standard deviation from three distinct measurements.

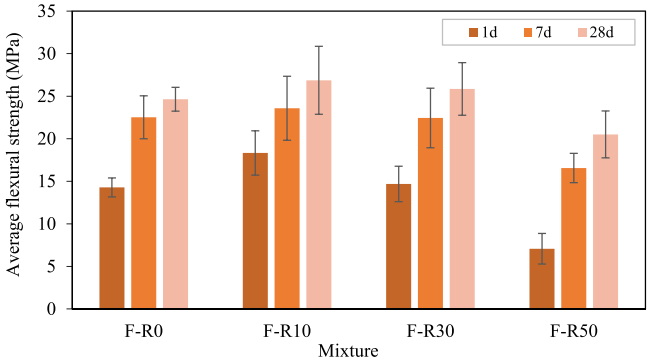

Fig. 15. Flexural strengths of the fiber-reinforced R-HPC mixtures with different replacement ratios tested at ages of 1, 7, and 28 days. The error bar represents the standard deviation from three distinct measurements.

3.1.5. Bond strength

The tensile bond strength of the FRHPC-NC composites was measured after 28 days of curing. All failures occurred along the interface making the failure stress representative of the actual tensile bond strength of the composites [63]. A typical post-mortem sample is presented in Fig. 19.

To quantify the impact of mRHPC replacement on the bond performance of the fiber-reinforced R-HPC repairs, the normalized tensile bond strengths were computed based on the reference tensile bond strength of 0.8 ± 0.1 MPa (F-R0 overlay). As shown in Fig. 20, the tensile bond strengths of the composites with R-HPC overlays were higher compared to that of the reference sample. Specifically, the application of the overlay modified with 30% mRHPC could provide a tensile bond strength 2.4 times that of the reference sample. To explain this result, it must be highlighted that in concrete-concrete composites, the overlay movement is mostly

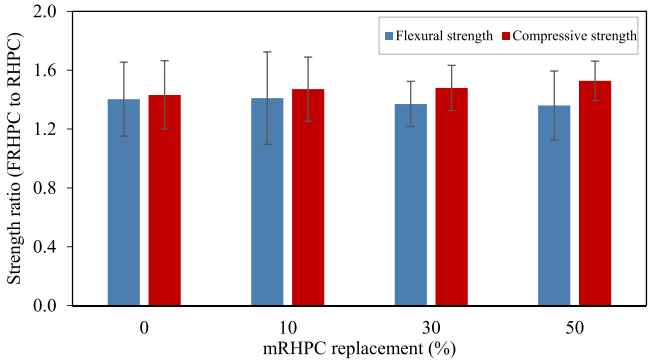

Fig. 16. Strength ratio of fiber-reinforced R-HPC to unreinforced R-HPC measured at 28 days.

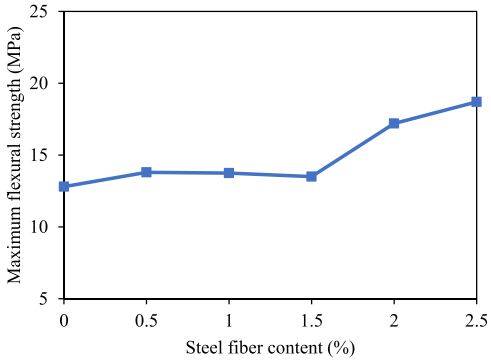

Fig. 17. Impacts of steel fiber content on the flexural strength of ultra-high performance cementitious composites after [61].

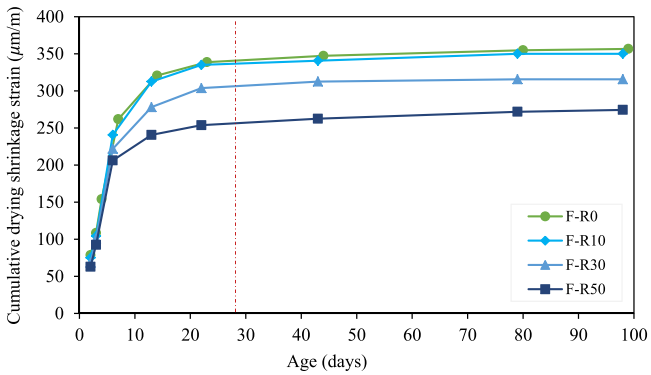

Fig. 18. Effect of mRHPC replacement percentage on the drying shrinkage value of the FRHPC specimens. The red dashed line highlights the drying shrinkage values at 28 days.

restrained by the substrate, and this restrained shrinkage is one of the primary causes of overlay cracking and interface debonding, and hence weak bond strength [35,64]. The present FRHPCs with 30% and 50% replacement rates did indeed exhibit lower drying shrinkage and should therefore induce lower stresses upon drying/setting. This will result in higher bond strength, as the current results confirm. The rheology of the fresh FRHPC may further enhance the benefits brought by mRHPC. Upon replacing OPC with mRHPC (50%), the funnel flow value decreased from 16 to 9 s and the slump flow value increased from 26 to 30 cm. This enhancement was consistent with the results of unreinforced samples and can be related to the mRHPC coarser particle size compared to the OPC, which reduces the amount of water required to wet the mRHPC, leading to a cement paste with higher fluidity. The remarkable changes in slump flow and funnel flow time could, in turn, result in a better spread on the substrate, filling the substrate surface texture, and hence improved anchorage. Nevertheless, it must be emphasized that the increase in bond strength results was higher than expected and this phenomenon should be further investigated.

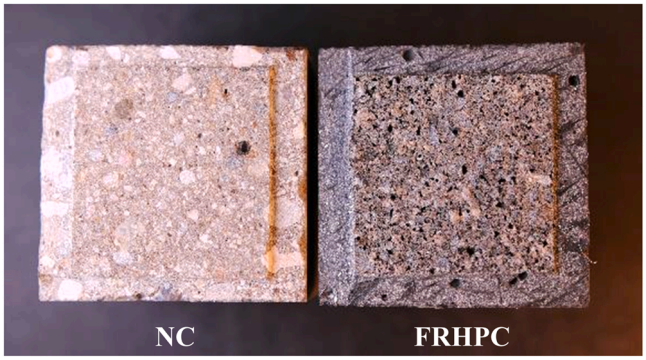

Fig. 19. Typical interfacial failure of FRHPC-NC specimens in the direct tension test. Fractured surface (interface) from the top view.

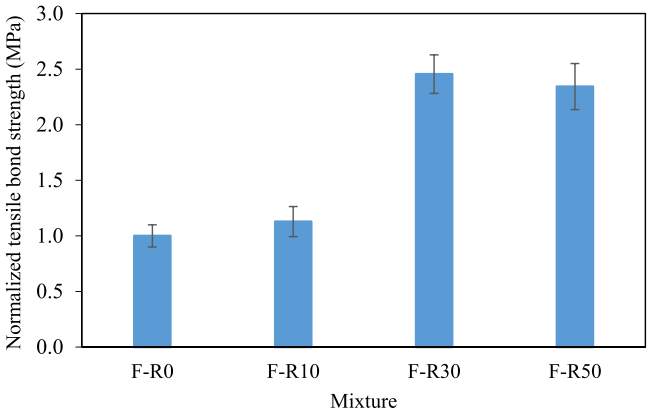

Fig. 20. Average tensile bond strengths of the FRHPC specimens tested after 28 days of curing. The error bar represents the standard deviation from three distinct measurements.

4. Conclusion

In this study, a novel sustainable binder made of milled recycled high-performance concrete (mRHPC) was proposed. A series of R-HPC mix designs was developed in which the ordinary Portland cement (OPC) was partially or fully replaced by mRHPC. To quantify its reactivity, linked to the cohesive forces developing upon hydration, the mRHPC powder was characterized using X-ray powder diffraction (XRPD), calorimetry and rheology (SAOS). The fresh and hardened state properties of the R-HPC mixtures were examined using mini slump flow cone, mini V-funnel flow, compressive and flexural strength measurements and shrinkage. The addition of 13 mm straight steel fibers was also investigated and composites of fiber-reinforced R-HPC overlays on NC substrates were prepared, targeting repair and strengthening applications. Based on the experimental results, the following conclusions were drawn:

- The mRHPC contained approximately 6.5 wt% of unhydrated clinker phases, explaining its residual reactivity.
- The early age structuration measured by small amplitude oscillatory rheology (SAOS) demonstrated a non-negligible structuration of mRHPC pastes (the storage modulus G′ reached 542 kPa after one hour, compared to 1560 kPa for OPC). The paste showed a clear hydration peak in the first 10 h, analogous to that of OPC, but with a lower heat rate (i.e., a cumulative heat of hydration of 23 J/g after 2 days versus 555 J/g for OPC).
- The specimens containing up to 30% mRHPC exhibited comparable compressive and flexural strengths to that of reference mixtures. Additionally, the fresh state characteristics (flowability and viscosity) of the mRHPC mixtures were unaffected or even improved.
- The mRHPC replacement did not reduce the beneficial effects of steel fibers. The use of 2% (by volume) steel fibers could provide the opportunity of extending the OPC replacement (up to 50%) with mRHPC while maintaining comparable mechanical properties.
- The drying shrinkage of the fiber-reinforced R-HPC samples decreased by up to 20% and the tensile bond strength of the steel fiber-reinforced overlay including 30% of mRHPC was 2.4 times that of the reference composites. The detrimental effect of restrained shrinkage on bond strength was therefore reduced upon using R-HPC overlays, explaining this remarkable result.

In conclusion, this work showed an opportunity to upcycle recycled HPC into a binder, addressing the challenge of accumulating demolished HPCs in the future. It also proposed SAOS rheological characterization, together with the widely accepted calorimetry

technique, to measure residual reactivity, a crucial feature to consider when using recycled materials as binders.

Declaration of Competing Interest

The authors declare that they have no known competing financial interests or personal relationships that could have appeared to influence the work reported in this paper.

Data Availability

Data will be made available on request.

References

[1] P.-C. Aïtcin, High performance concrete, 1998. https://doi.org/10.14359/4167.
[2] M. Schmidt, E. Fehling, Ultra-high-performance concrete: research, development and application in Europe, Am. Concr. Inst. Acids Spec. Publ. SP-228 (2005) 51–77.
[3] A. Neville, P.C. Aïtcin, High performance concrete - an overview, Mater. Struct. Constr. 31 (1998) 111–117, https://doi.org/10.1007/bf02486473.
[4] J. Li, Z. Wu, C. Shi, Q. Yuan, Z. Zhang, Durability of ultra-high performance concrete – a review, Constr. Build. Mater. 255 (2020), 119296, https://doi.org/10.1016/j.conbuildmat.2020.119296.
[5] C. Shi, Z. Wu, J. Xiao, D. Wang, Z. Huang, Z. Fang, A review on ultra high performance concrete: Part I. Raw materials and mixture design, Constr. Build. Mater. 101 (2015) 741–751, https://doi.org/10.1016/j.conbuildmat.2015.10.088.
[6] A.K. Akhnoukh, C. Buckhalter, Ultra-high-performance concrete: constituents, mechanical properties, applications and current challenges, Case Stud. Constr. Mater. 15 (2021), e00559, https://doi.org/10.1016/j.cscm.2021.e00559.
[7] Z. Wu, C. Shi, W. He, L. Wu, Effects of steel fiber content and shape on mechanical properties of ultra high performance concrete, Constr. Build. Mater. 103 (2016) 8–14, https://doi.org/10.1016/j.conbuildmat.2015.11.028.
[8] S. Abbas, A.M. Soliman, M.L. Nehdi, Exploring mechanical and durability properties of ultra-high performance concrete incorporating various steel fiber lengths and dosages, Constr. Build. Mater. 75 (2015) 429–441, https://doi.org/10.1016/j.conbuildmat.2014.11.017.
[9] N.M. Azmee, N. Shafiq, Ultra-high performance concrete: from fundamental to applications, Case Stud. Constr. Mater. 9 (2018), https://doi.org/10.1016/j.cscm.2018.e00197.
[10] M. Dan Gavriletea, Environmental impacts of sand exploitation. Analysis of sand market, Sustain 9 (2017), https://doi.org/10.3390/su9071118.
[11] L. Koehnken, M. Rintoul, Impacts of sand mining on ecosystem structure, process & biodiversity in rivers, World Wildl. Fund. Int. (2018). ⟨moz-extension://8ad02336-52ad-4304-9c7e-e6c9af118709/enhanced-reader.html?openApp&pdf=http%3A%2F%2Fd2ouvy59p0dg6k.cloudfront.net%2Fdownloads%2Fsand_mining_impacts_on_world_rivers_final_.pdf⟩.
[12] U.S. Geological Survey, Mineral commodity summaries 2020: U.S. Geological Survey, 2020.
[13] D.L. Summerbell, C.Y. Barlow, J.M. Cullen, Potential reduction of carbon emissions by performance improvement: a cement industry case study, J. Clean. Prod. 135 (2016) 1327–1339, https://doi.org/10.1016/j.jclepro.2016.06.155.
[14] WBCSD, IEA, Cement Technology Roadmap 2009: Carbon emissions reductions up to 2050, 2009.
[15] P. Villoria Sáez, M. Osmani, A diagnosis of construction and demolition waste generation and recovery practice in the European Union, J. Clean. Prod. 241 (2019), https://doi.org/10.1016/j.jclepro.2019.118400.
[16] A. Di Maria, J. Eyckmans, K. Van Acker, Downcycling versus recycling of construction and demolition waste: combining LCA and LCC to support sustainable policy making, Waste Manag 75 (2018) 3–21, https://doi.org/10.1016/j.wasman.2018.01.028.
[17] E.A. Ohemeng, S.O. Ekolu, Comparative analysis on costs and benefits of producing natural and recycled concrete aggregates: a South African case study, Case Stud. Constr. Mater. 13 (2020), e00450, https://doi.org/10.1016/j.cscm.2020.e00450.
[18] The European Commission, Directive (EU) 2018/851 of the European Parliament and of the Council of 30 May 2018, Off. J. Eur. Union. L312 (2008) 1–59. ⟨http://eur-lex.europa.eu/LexUriServ/LexUriServ.do?uri=OJ:L:2008:312:0003:01:ES:HTML⟩.
[19] S. Singh, R. Nagar, V. Agrawal, A. Rana, A. Tiwari, Sustainable utilization of granite cutting waste in high strength concrete, J. Clean. Prod. 116 (2016) 223–235, https://doi.org/10.1016/j.jclepro.2015.12.110.
[20] G. Andreu, E. Miren, Experimental analysis of properties of high performance recycled aggregate concrete, Constr. Build. Mater. 52 (2014) 227–235, https://doi.org/10.1016/j.conbuildmat.2013.11.054.
[21] M.C. Limbachiya, T. Leelawat, R.K. Dhir, Use of recycled concrete aggregate in high-strength concrete, Mater. Struct. Constr. 33 (2000) 574–580, https://doi.org/10.1007/bf02480538.
[22] S. Kox, G. Vanroelen, J. Van Herck, H. de Krem, B. Vandoren, Experimental evaluation of the high-grade properties of recycled concrete aggregates and their application in concrete road pavement construction, Case Stud. Constr. Mater. 11 (2019), e00282, https://doi.org/10.1016/j.cscm.2019.e00282.
[23] D. Castillo, J.C. Cruz, D.L. Trejo-arroyo, E.M. Muzquiz, Z. Zarhri, Case studies in construction materials characterization of poultry litter ashes as a supplementary cementitious material, Case Stud. Constr. Mater. 17 (2022), e01278, https://doi.org/10.1016/j.cscm.2022.e01278.
[24] D.M. Kannan, S.H. Aboubakr, A.S. EL-Dieb, M.M.Reda Taha, High performance concrete incorporating ceramic waste powder as large partial replacement of Portland cement, Constr. Build. Mater. 144 (2017) 35–41, https://doi.org/10.1016/j.conbuildmat.2017.03.115.
[25] M.H. Zhang, V.M. Malhotra, High-performance concrete incorporating rice husk ash as a supplementary cementing material, Acids Mater. J. 93 (1996) 629–636, https://doi.org/10.14359/9870.
[26] M.A. Megat Johari, J.J. Brooks, S. Kabir, P. Rivard, Influence of supplementary cementitious materials on engineering properties of high strength concrete, Constr. Build. Mater. 25 (2011) 2639–2648, https://doi.org/10.1016/j.conbuildmat.2010.12.013.
[27] D. Pedro, J. de Brito, L. Evangelista, Mechanical characterization of high performance concrete prepared with recycled aggregates and silica fume from precast industry, J. Clean. Prod. 164 (2017) 939–949, https://doi.org/10.1016/j.jclepro.2017.06.249.
[28] D. Pedro, J. de Brito, L. Evangelista, Durability performance of high-performance concrete made with recycled aggregates, fly ash and densified silica fume, Cem. Concr. Compos. 93 (2018) 63–74, https://doi.org/10.1016/j.cemconcomp.2018.07.002.
[29] J.A. Bogas, J. De Brito, D. Ramos, Freeze-thaw resistance of concrete produced with fine recycled concrete aggregates, J. Clean. Prod. 115 (2016) 294–306, https://doi.org/10.1016/j.jclepro.2015.12.065.
[30] J.A. Bogas, A. Carriço, M.F.C. Pereira, Mechanical characterization of thermal activated low-carbon recycled cement mortars, J. Clean. Prod. 218 (2019) 377–389, https://doi.org/10.1016/j.jclepro.2019.01.325.
[31] H. Krour, R. Trauchessec, A. Lecomte, C. Diliberto, L. Barnes-Davin, B. Bolze, A. Delhay, Incorporation rate of recycled aggregates in cement raw meals, Constr. Build. Mater. 248 (2020), 118217, https://doi.org/10.1016/j.conbuildmat.2020.118217.
[32] J.A. Bogas, A. Carriço, S. Real, Durability of concrete produced with recycled cement from waste concrete, Mater. Today Proc. 58 (2022) 1149–1154, https://doi.org/10.1016/j.matpr.2022.01.280.
[33] S. Li, J. Gao, Q. Li, X. Zhao, Investigation of using recycled powder from the preparation of recycled aggregate as a supplementary cementitious material, Constr. Build. Mater. 267 (2021), 120976, https://doi.org/10.1016/j.conbuildmat.2020.120976.

[34] R.V. Silva, J. De Brito, R.K. Dhir, Prediction of the shrinkage behavior of recycled aggregate concrete: a review, Constr. Build. Mater. 77 (2015) 327–339, https://doi.org/10.1016/j.conbuildmat.2014.12.102.
[35] D. Daneshvar, K. Deix, A. Robisson, B. Shafei, Investigation of drying shrinkage effects on sloped concrete-concrete composites, Comput. Model. Concr. Concr. Struct. (2022) 634–639, https://doi.org/10.1201/9781003316404-75.
[36] N. Van Tuan, G. Ye, K. Van Breugel, O. Copuroglu, Hydration and microstructure of ultra high performance concrete incorporating rice husk ash, Cem. Concr. Res. 41 (2011) 1104–1111, https://doi.org/10.1016/j.cemconres.2011.06.009.
[37] Y. Shi, G. Long, X. Zeng, Y. Xie, H. Wang, Green ultra-high performance concrete with very low cement content, Constr. Build. Mater. 303 (2021), 124482, https://doi.org/10.1016/j.conbuildmat.2021.124482.
[38] B.A. Tayeh, B.H. Abu Bakar, M.A. Megat Johari, Y.L. Voo, Mechanical and permeability properties of the interface between normal concrete substrate and ultra high performance fiber concrete overlay, Constr. Build. Mater. 36 (2012) 538–548, https://doi.org/10.1016/j.conbuildmat.2012.06.013.
[39] Y. Zhang, C. Zhang, Y. Zhu, J. Cao, X. Shao, An experimental study: various influence factors affecting interfacial shear performance of UHPC-NSC, Constr. Build. Mater. 236 (2020), 117480, https://doi.org/10.1016/j.conbuildmat.2019.117480.
[40] B.A. Tayeh, B.H. Abu Bakar, M.A.Megat Johari, Characterization of the interfacial bond between old concrete substrate and ultra high performance fiber concrete repair composite, Mater. Struct. Constr. 46 (2013) 743–753, https://doi.org/10.1617/s11527-012-9931-1.
[41] Z. He, X. Zhu, J. Wang, M. Mu, Y. Wang, Comparison of CO 2 emissions from OPC and recycled cement production, Constr. Build. Mater. 211 (2019) 965–973, https://doi.org/10.1016/j.conbuildmat.2019.03.289.
[42] S. Wang, H. Zhu, F. Liu, S. Cheng, B. Wang, L. Yang, Effects of steel fibers and concrete strength on flexural toughness of ultra-high performance concrete with coarse aggregate, Case Stud. Constr. Mater. 17 (2022), e01170, https://doi.org/10.1016/j.cscm.2022.e01170.
[43] Victor C. Li, On engineered cementitious composites (ECC): a review of the material and its applications, J. Adv. Concr. Technol. 1 (2003) 215–230.
[44] B. Chun, S. Kim, D.Y. Yoo, Reinforcing effect of surface-modified steel fibers in ultra-high-performance concrete under tension, Case Stud. Constr. Mater. 16 (2022), e01125, https://doi.org/10.1016/j.cscm.2022.e01125.
[45] A. Behnood, K. Van Tittelboom, N. De Belie, Methods for measuring pH in concrete: a review, Constr. Build. Mater. 105 (2016) 176–188, https://doi.org/10.1016/j.conbuildmat.2015.12.032.
[46] P. Faucon, F. Adenot, M. Jorda, R. Cabrillac, Behaviour of crystallised phases of Portland cement upon water attack, Mater. Struct. Constr. 30 (1997) 480–485, https://doi.org/10.1007/bf02524776.
[47] C.Feng Lu, W. Wang, Q. tao Li, M. Hao, Y. Xu, Effects of micro-environmental climate on the carbonation depth and the pH value in fly ash concrete, J. Clean. Prod. 181 (2018) 309–317, https://doi.org/10.1016/j.jclepro.2018.01.155.
[48] H.F. Taylor, Cement chemistry, 1997. https://doi.org/10.1016/s0958–9465(98)00023–7.
[49] M. Bellotto, Cement paste prior to setting: A rheological approach, Cem. Concr. Res. 52 (2013) 161–168, https://doi.org/10.1016/j.cemconres.2013.07.002.
[50] L. Nachbaur, J.C. Mutin, A. Nonat, L. Choplin, Dynamic mode rheology of cement and tricalcium silicate pastes from mixing to setting, Cem. Concr. Res. 31 (2001) 183–192, https://doi.org/10.1016/S0008-8846(00)00464-6.
[51] Q. Yuan, X. Lu, K.H. Khayat, D. Feys, C. Shi, Small amplitude oscillatory shear technique to evaluate structural build-up of cement paste, Mater. Struct. Constr. 50 (2017) 1–12, https://doi.org/10.1617/s11527-016-0978-2.
[52] T. Liberto, M. Bellotto, A. Robisson, Small oscillatory rheology and cementitious particle interactions, Cem. Concr. Res. 157 (2022), 106790, https://doi.org/10.1016/j.cemconres.2022.106790.
[53] S. Ma, Y. Qian, S. Kawashima, Experimental and modeling study on the non-linear structural build-up of fresh cement pastes incorporating viscosity modifying admixtures, Cem. Concr. Res. 108 (2018) 1–9, https://doi.org/10.1016/j.cemconres.2018.02.022.
[54] A.M. Mostafa, A. Yahia, New approach to assess build-up of cement-based suspensions, Cem. Concr. Res. 85 (2016) 174–182, https://doi.org/10.1016/j.cemconres.2016.03.005.
[55] R.G. Larson, The Structure and Rheology of Complex Fluids, Oxford University Press, 1999.
[56] E.M. Gartner, J.F. Young, D.A. Damidot, I. Jawed, Hydration of Portland Cement, Struct. Perform. Cem. (2002) 57–113.
[57] H.M. Jennings, Model for the microstructure of calcium silicate hydrate in cement paste, Cem. Concr. Res. 30 (2000) 101–116, https://doi.org/10.1016/S0008-8846(99)00209-4.
[58] J.F. Munoz and I. De la Varga, Ultra-High Performance Concrete for Bridge Deck Overlays, 2018. ⟨https://www.fhwa.dot.gov/publications/research/infrastructure/bridge/17097/index.cfm⟩.
[59] L.J. Murdock, The workability of concrete, Mag. Concr. Res. 12 (1960) 135–144, https://doi.org/10.1680/macr.1961.13.38.79.
[60] M. Maage, Interaction between steel fibers and cement based matrixes, Matér. Constr. 10 (1977) 297–301, https://doi.org/10.1007/BF02478831.
[61] G.M. Ren, H. Wu, Q. Fang, J.Z. Liu, Effects of steel fiber content and type on static mechanical properties of UHPCC, Constr. Build. Mater. 163 (2018) 826–839, https://doi.org/10.1016/j.conbuildmat.2017.12.184.
[62] N.P. Tran, C. Gunasekara, D.W. Law, S. Houshyar, S. Setunge, A. Cwirzen, A critical review on drying shrinkage mitigation strategies in cement-based materials, J. Build. Eng. 38 (2021), 102210, https://doi.org/10.1016/j.jobe.2021.102210.
[63] D. Daneshvar, K. Deix, A. Robisson, Effect of casting and curing temperature on the interfacial bond strength of epoxy bonded concretes, Constr. Build. Mater. 307 (2021), 124328, https://doi.org/10.1016/j.conbuildmat.2021.124328.
[64] H. Beushausen, M.G. Alexander, Failure mechanisms and tensile relaxation of bonded concrete overlays subjected to differential shrinkage, Cem. Concr. Res. 36 (2006) 1908–1914, https://doi.org/10.1016/j.cemconres.2006.05.027.